CHAPTER 1

THEORY OF OPERATIONS

In this section, the aforementioned multi-frequency approaches will be developed to transfer wired and wireless power concurrently, which can be applied for wireless power transfer based contactless slip rings (WPT-CSRs) using just a single converter of the motor drives. Since the motor drives require a dynamic operation, which should have a fast response, their conventional modulation techniques should be used. Therefore, it is challenging to achieve the continuous power transfer of WPT-CSRs under any motor operations during these modulation techniques.

In this study, two methods that control the power of WPT-CSR will be presented for DC and AC motors, and the theory of the proposed system will be investigated systematically. Firstly, the proposed WPT-CSR is introduced and compared with conventional ones. Secondly, conventional motor drives are presented, and the voltage source converters are examined. Thirdly, DC motor drives are investigated. Their speed/torque control and applied modulation techniques are discussed. In addition, the proposed control method, which concurrently drives the motor and excites WPT-CSR, is introduced. Fourthly, AC motor drives are investigated similarly to DC motor drives. Fifthly, the current PWM techniques for conventional DC and AC motor drives are discussed. Finally, practical considerations of employing the proposed system in the conventional drives are investigated, and the importance of wide-bandgap switches is examined.

1.1 The Proposed Contactless Slip Ring

A conventional WPT-CSR is shown in Fig. 1.1.a. The already existing motor drive in these systems generates high-frequency switching voltage harmonics, which are not desired, and attenuated in the motor phase currents due to high motor inductance. Such systems consist of two separate converters to drive the motor and excite the WPT system. In the proposed system, the Tx coil utilizes these high-frequency

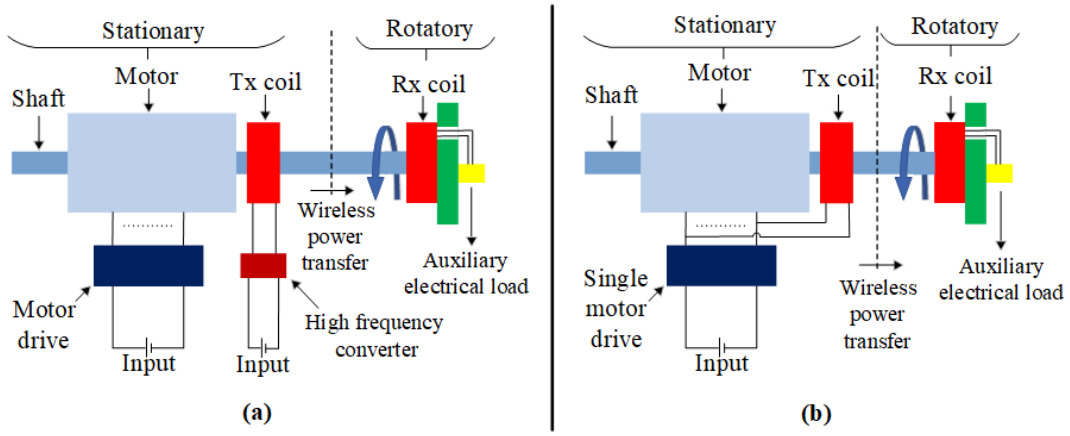

Figure 1.1: An example representation of the proposed CSRs based on WPT system for rotating frames. a) Conventional Systems. b) The proposed system.

voltage harmonics to transfer power to the Rx coil on the rotating frame, while the low-frequency modulated current is still used to drive the motor. Thus, a separate WPT converter is no longer required. In other words, a motor and a WPT-CSRs are driven concurrently by a single converter, as shown in Fig. 1.1.b. Thus, the converter of the motor drive is used as the single converter by the multi-frequency approaches discussed in the previous section, and the high-frequency converter of the WPT system is eliminated, reducing the cost and complexity. The proposed system can be used to energize auxiliary loads in the rotating frame for industrial applications such as IoT devices, surveillance cameras, robotic actuators, radars, sensors, etc., or excite the field windings of the synchronous motors. Since the power ratings of these loads are lower than the power ratings of the motor, it is possible to use the existing conventional motor drive, which will be discussed in the coming parts, without any hardware modifications.

1.2 Motor Drives

Motor drives have gained popularity in industrial applications. They are frequently used in the production phases, such as robotic arms and conveyor belts, in the consumer products, such as electric vehicles (EVs), and in renewable energy sources, such as wind turbines. Considering the types of motors, they can be divided into two main types: DC and AC drives. DC motor drives adjust the DC voltage/current to control the speed and torque of motors. Unlike DC motor drives, AC motor drives also adjust the frequency to control the speed of motors; thus, AC motor drives are also named variable frequency drives (VFDs). As shown in Fig. 1.2, motor drives generally comprise a measurement unit, controller, and DC/DC or DC/AC converter.

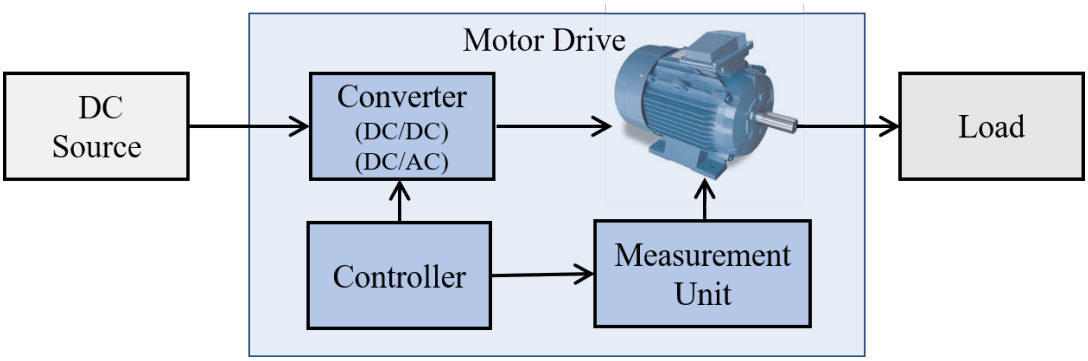

Figure 1.2: Block diagram of a conventional motor drive system.

These converters can be the current source (CSC) or voltage source converters (VSC). While VSCs commonly use MOSFETs and IGBTs that block voltage in one direction, CSCs use diodes and thyristors that pass the current in one direction. VSCs generate a pulsating output voltage under constant input voltage, and their output voltage is independent of loading. On the contrary, CSCs generate a pulsating output current under constant input current, and their output current is independent of loading. In this study, VSC-based motor drives are used to achieve independent output voltage from the loading of the motor and the WPT-CSR, so the WPT-CSR can be connected parallel to the motor.

1.3 DC motor drives

There are two main parts in DC motors: field and armature. The field is on the stationary part while the armature is on the rotating frame. According to the excitation of field windings, DC machines are divided into four main types: series, shunt, compound, and separately excited. The field and armature windings in series-DC machines are series-connected, meaning their currents are equal. If the windings are connected to parallel, meaning their voltages are equal, the machines are called shunt-DC machines. DC machines having combined series and shunt field windings are called compound-DC machines. Lastly, in separately excited-DC machines, field and armature windings are independently fed. For applications requiring sensitive speed and torque control, separately excited machines are generally preferred, and they can be controlled via armature voltage and field current. In this part, the proposed system will be investigated for implementation with separately excited DC machines as an example case. Their implementation and control will be investigated. However, the methodology can be easily applied to other types of DC machines.

1.3.1 Speed and Torque Control

The equivalent circuit schematic of a separately excited-DC machine is presented in Fig. 1.3.

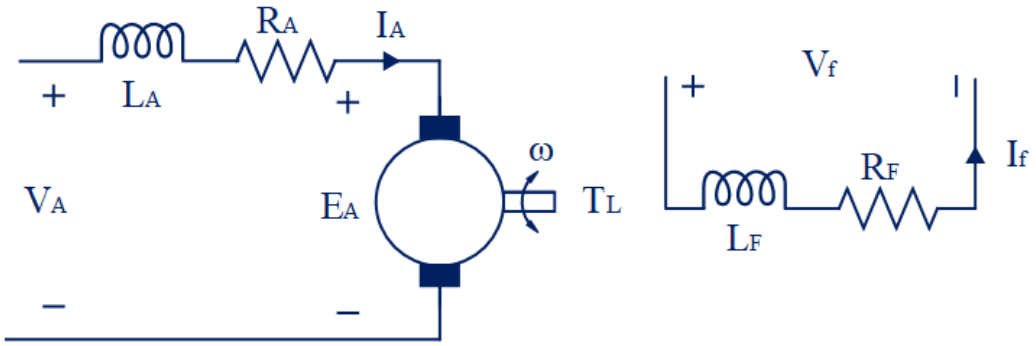

Figure 1.3: The electrical equivalent circuit schematic of the separately excited DC motor.

The induced emf on the armature (E_A) is proportional to speed, calculated as in (1.1),

where K_A is the motor back-emf constant.

$$E_A = K_A \omega \tag{1.1}$$

The torque is proportional to the current, as calculated in (1.2).

$$T = K_A I_A \tag{1.2}$$

Therefore, in order to achieve the desired speed and torque references, the current and induced emf should be controlled. The control can be provided with armature voltage under constant field excitation (and constant K_A). Moreover, in order to increase high-speed performance, the field current can be controlled, which changes K_A. The control block diagram of conventional DC motor drives is presented in Fig. 1.4.

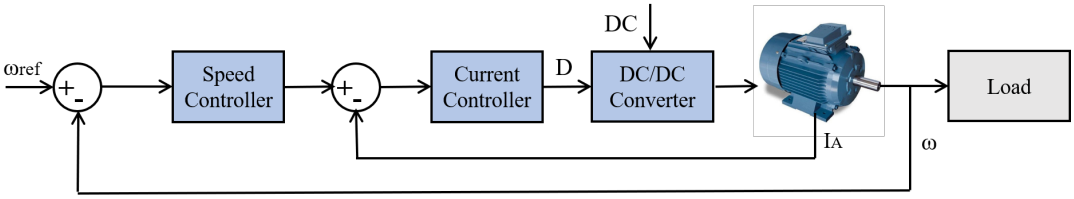

Figure 1.4: The control diagram of conventional DC motor drives.

This required armature voltage can be supplied using VSCs, governed by modulation techniques that generate a pulsating output voltage.

1.3.2 Applied Modulation Techniques

In the previous part, a required armature voltage of the motor is found considering the desired speed and torque references. This voltage can be produced using a full-bridge VSC, shown in Fig. 1.5. The converter is driven by a bipolar pulse width modulation (PWM) technique, as given in Fig. 1.6, which generates DC output voltage with high-frequency switching harmonics. In this modulation technique, S_A and $S_B^{'}$ (hence S_B-$S_A^{'}$) have the same switching patterns. The switching function of the applied PWM is presented in (1.3), composed of switching frequency (f_s), and duty cycle (D). The harmonic distribution of the converter output voltage for this PWM is given in Fig. 1.7.

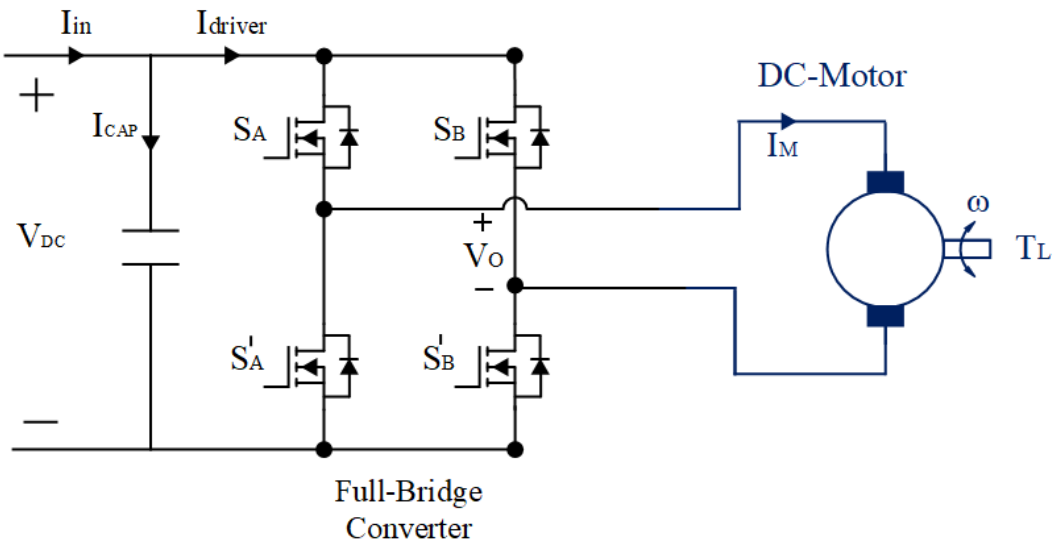

Figure 1.5: The circuit diagram of a full-bridge VSC DC motor drive.

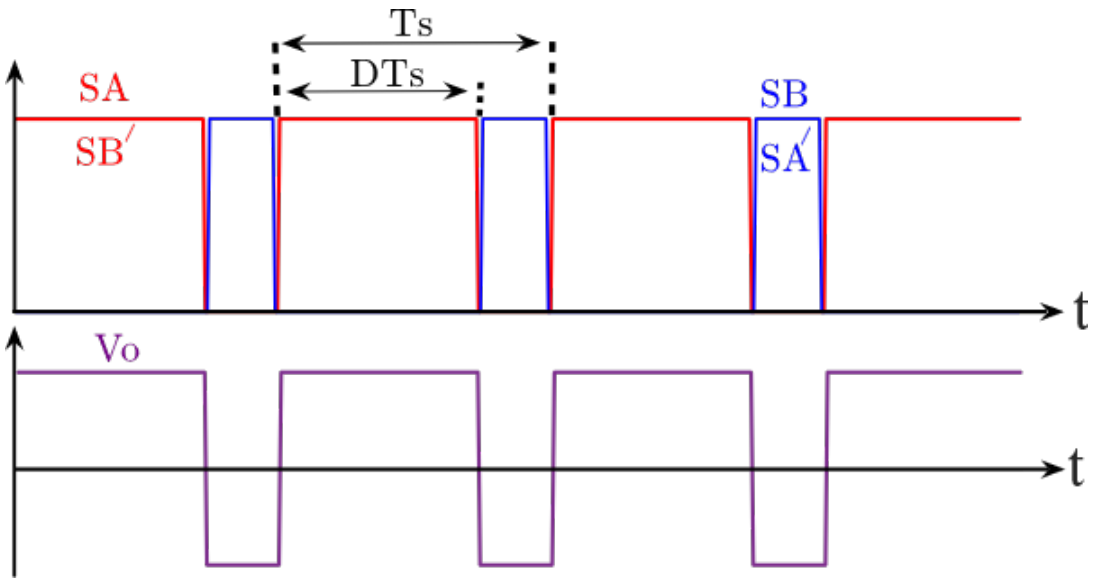

Figure 1.6: The switching signals and output voltage of the full-bridge VSC.

$$S(t) = \mathrm{D} + \sum_{\mathrm{k}=1}^{\infty} \frac{2}{\mathrm{k}\pi} \sin(\mathrm{k}\pi\mathrm{D}) \cos(2\pi \mathrm{k} \mathrm{f_s} \mathrm{t}) \tag{1.3}$$

While a positive DC output voltage is achieved for duty cycle (D) values greater than 0.5, a negative DC output voltage is achieved for D values less than 0.5. At $D = 0.5$, the DC output becomes zero, meaning that the power transferred to the motor is zero. Therefore, positive and negative DC output voltage levels can be obtained by varying

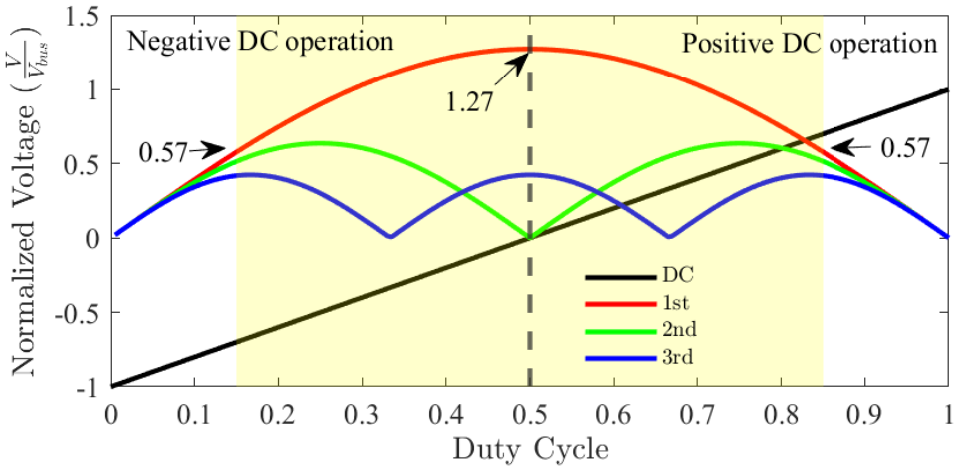

Figure 1.7: The harmonic distribution of the converter's output voltage, which are obtained by analytically employing the switching function in the FB converter.

the D. This modulation technique can control the motor speed, torque, and rotation direction.

1.3.3 Control Methodology for the proposed system

In the proposed system, the WPT-CSR is connected in parallel to the DC motor as presented in Fig. 1.8, and a full-bridge VSC, which bipolar PWM drives, is used. According to the harmonic distribution of the converter output voltage, presented in Fig. 1.7, while the duty cycle controls the torque and speed of the motor, the switching frequency, and its harmonics also vary with the duty cycle. In the proposed system, the resonant frequency of the WPT-CSR is selected close to the switching frequency so that it can excite the WPT-CSR. However, there are two main problems. Firstly, at duty cycles close to 0 or 1, the switching harmonics are diminished and converged to 0. Thus, the operational duty cycle range should be restricted to achieve continuous power transfer using these harmonics. For example, the restricted operational duty cycles, highlighted in yellow (between 0.15 and 0.85), are shown in Fig. 1.7. In this situation, DC-link utilization is reduced, but a similar restriction already exists in conventional drives due to the dead times. Secondly, varying duty cycles also affect the transferred power by the WPT-CSR. This power should be independently controlled, and the system should operate under different motor operations (different

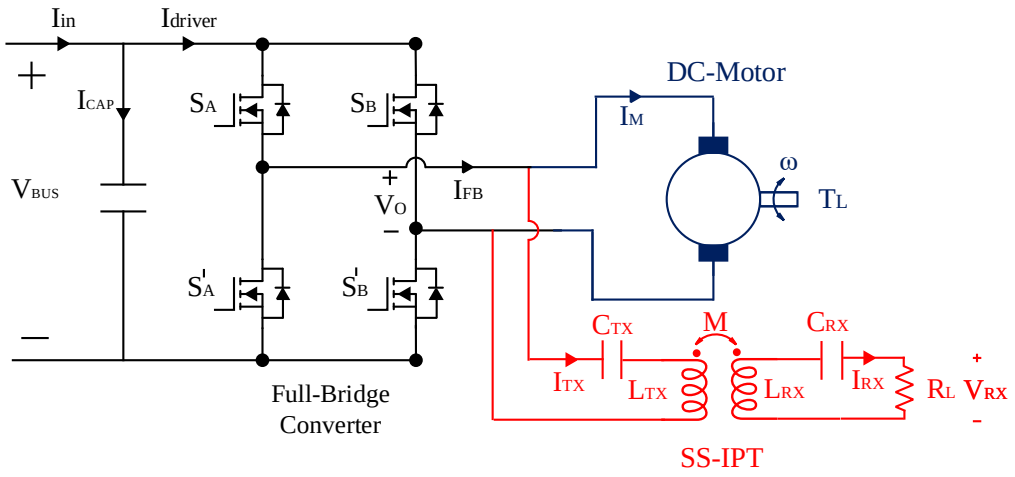

Figure 1.8: Circuit diagram of the proposed concurrent motor drive and WPT systems with a single converter.

duty cycles). This problem can be solved with two different methods. One is to add post-regulation with an active converter to the receiver side rather than using a passive full-bridge diode rectifier, but it increases the cost, complexity, and weight of the rotating side. Another is frequency detuning control, commonly used in WPT systems. Since the motor winding attenuates the high-frequency harmonics in motor current, the variable switching frequency does not affect the motor operation. Thus, the variable switching frequency can be applied to the motor drives to control the WPT-CSR power. Consequently, the overall control diagram for the proposed system is given in Fig. 1.9. The motor controller decides on the duty cycle, considering the desired speed and torque references. Then, the WPT-CSR controller adjusts the switching frequency to obtain the desired WPT-CSR output power for these different motor operations.

A steady-state expected voltage and current waveforms for an operation point are given Fig. 1.10 where the gate signals of the top switches of each leg (S_A and S_B) are shown. The switching pattern generates a pulsating output voltage (V_o), with a DC and switching components. The motor current (I_M) is mainly DC with small current ripples. The Tx current (I_{TX}) is sinusoidal, assuming that WPT-CSR has a high-quality factor. The FB converter current (I_{FB}) is the sum of I_M and I_{TX}. However,

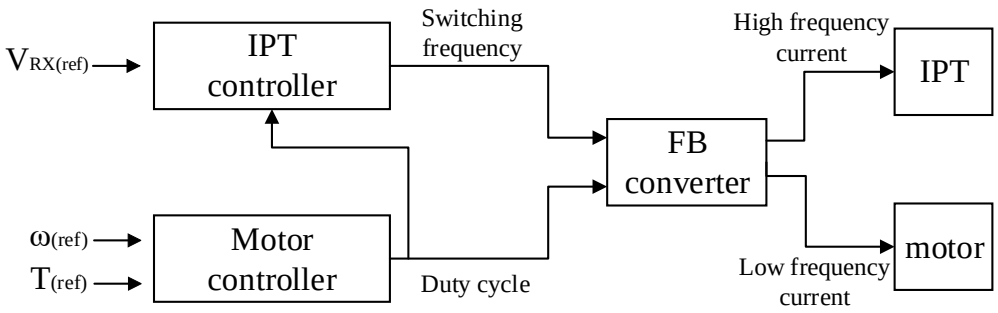

Figure 1.9: The block diagram of the control method of the combined motor and IPT system.

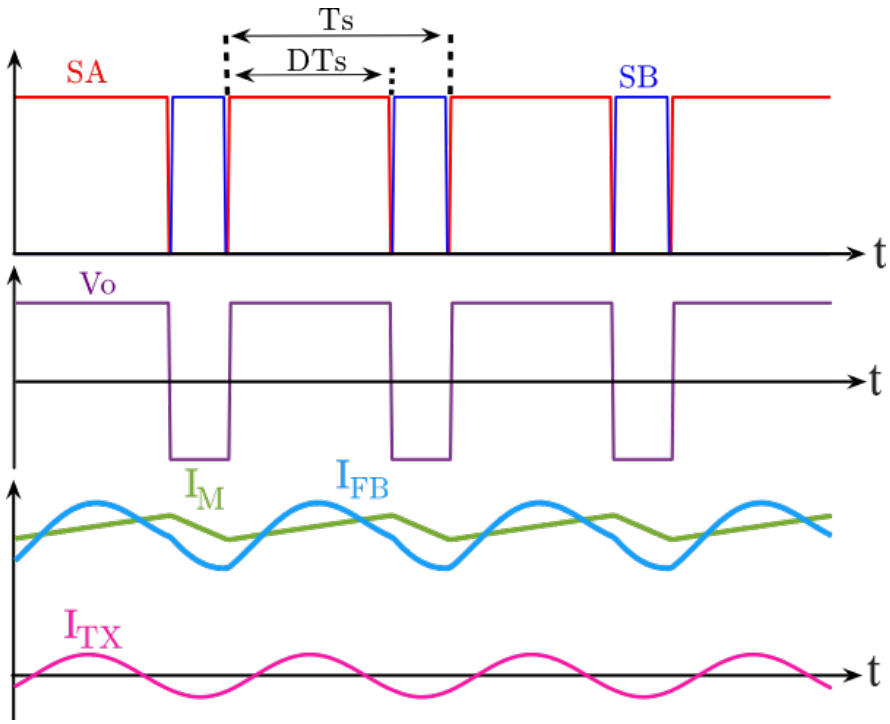

Figure 1.10: Asymmetrical PWM signals and its corresponding voltage and current waveforms.

I_{FB} is dominated by I_M since the WPT-CSR system is used for auxiliary systems with smaller power ratings than the motor.

1.4 AC Motor Drives

There are two main parts in AC machines: field and armature. According to the AC machines type, the method of field excitation changes. For induction machines (IMs), the field on the rotor is fed by induction; there is no requiring external excitation. Their armature on the stator is fed with AC voltages, and the rotating magnetic field generated by the armature induces a voltage on the field windings. So, IMs have a simple structure without brushes or permanent magnets on the rotating frame, making them robust. Accordingly, the control of IMs is achieved using AC excitation with variable frequency and magnitude to just the armature windings. In synchronous machines (SMs), the field winding is on the rotor and excited by DC voltage (or permanent magnets can be used to excite), while the armature winding on the stator is fed with AC voltage. Unlike IMs, the control of SMs can be achieved by both field control (with DC voltage/current) and armature control (with variable frequency, phase angle, and magnitude of AC voltages). However, field control does not regulate the speed of the motor, and it is usually used to increase high-speed performance. Consequently, AC motor drives are supposed to generate variable frequency output voltages, which feed the armatures of AC machines. There are other types of AC machines, but in this study, SMs and IMs are investigated to implement the proposed system, and the proposed methods can also be easily implemented in other AC machines.

1.4.1 Speed and Torque Control

The speed of the stator excitation is called synchronous speed. IMs do not operate at synchronous speed, so the rotor mechanical speed should differ from the synchronous speed to achieve net torque.

The difference between the rotor and synchronous speed per unit is called slip. This slip is required in order to excite the field by induction. The torque-speed characteristic of IMs and their electrical equivalent circuit is shown in Fig. 1.11 and Fig. 1.12.

The generated torque can be calculated as given in (1.4) where R_2^r and X_2^r is reflected

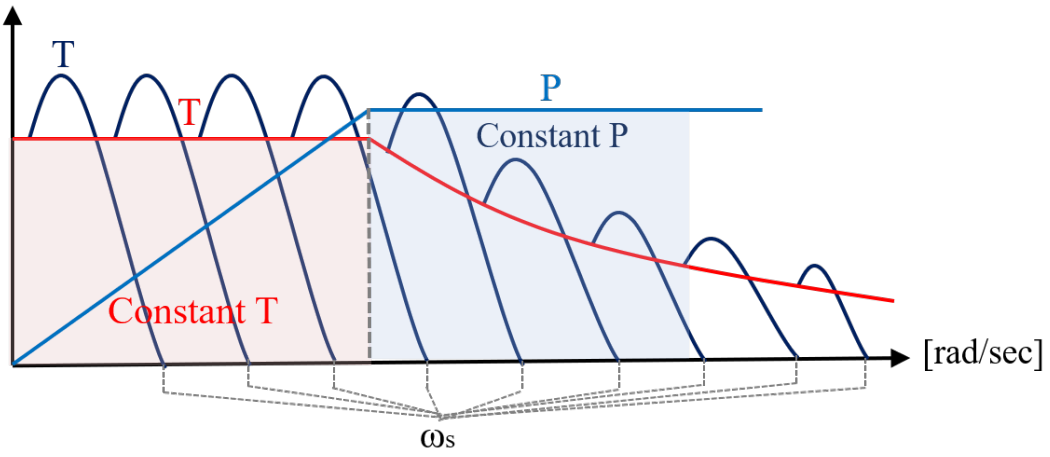

Figure 1.11: Torque-speed characteristic of IMs. (ω_s is synchronous speed, P and T are power and torque respectively.)

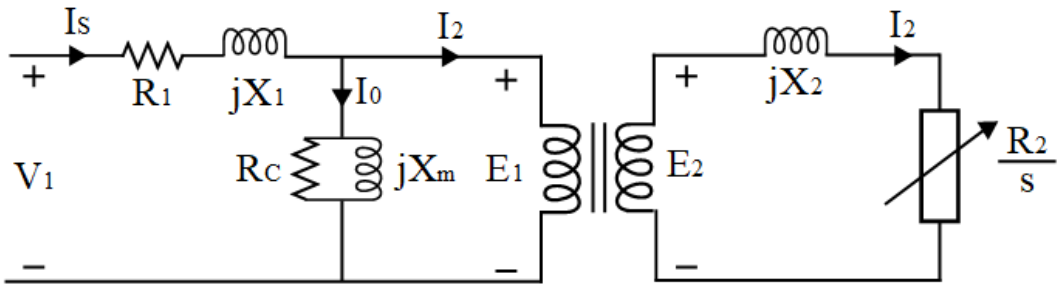

Figure 1.12: Electrical equivalent circuit of IMs

resistance and impedance.

$$T = \frac{3V_1^2}{(R_1 + \frac{R_2^r}{s})^2 + (X_1 + X_2^r)^2} \frac{R_2^r}{s\omega_s} \tag{1.4}$$

The rotor speed is calculated using s and ω_S as given in (1.5).

$$\omega_r = (1 - s)\omega_s \tag{1.5}$$

On the contrary, SMs operate at synchronous speed. Therefore, the mechanical speed is directly controlled by the electrical frequency. The torque is adjusted by the armature current controlled by the applied armature voltage. Moreover, the field current can be controlled to obtain high-speed performance. The torque-speed characteristic of SMs and their electrical equivalent circuit is shown in Fig. 1.13 and Fig. 1.14.

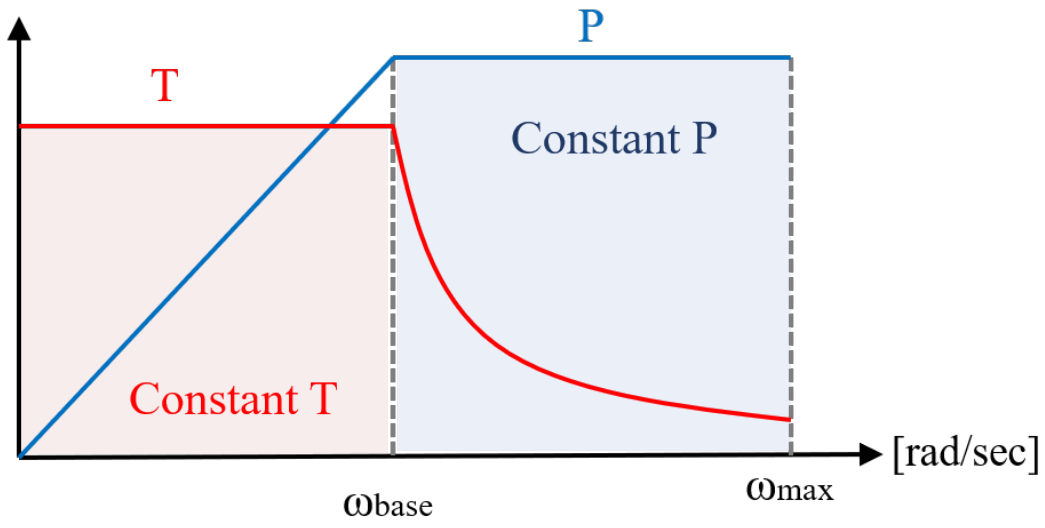

Figure 1.13: Torque-speed characteristic of IMs

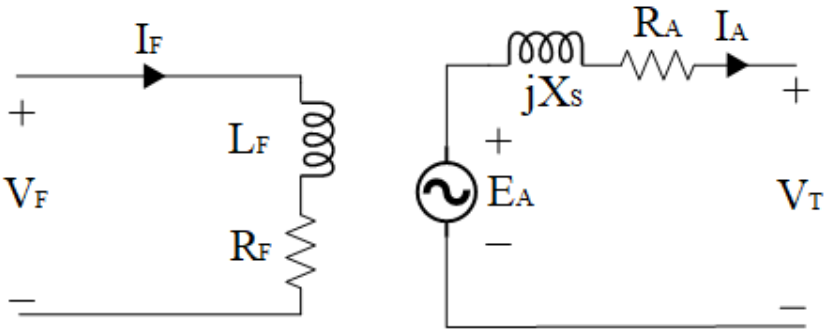

Figure 1.14: Electrical equivalent circuit of IMs

The induced emf on the AC motor is proportional to the speed of the motor, calculated as in (1.6) where K is the motor back-emf constant that depends on the field.

$$E_A = K\omega_s \tag{1.6}$$

The armature current in phasor domain is calculated as given in (1.7).

$$\overrightarrow{I_a} = \frac{\overrightarrow{V_t} - \overrightarrow{E_A}}{R_a + jX_s} \tag{1.7}$$

The motor operates at synchronous speed, and its torque is calculated as given in (1.8).

$$T_e = 3\frac{\overrightarrow{E_f}\,\overrightarrow{I_a}}{\omega_s} \tag{1.8}$$

Therefore, in order to achieve the desired speed and torque references, the armature voltages should be controlled. The control block diagram of AC machines is presented in Fig. 1.15.

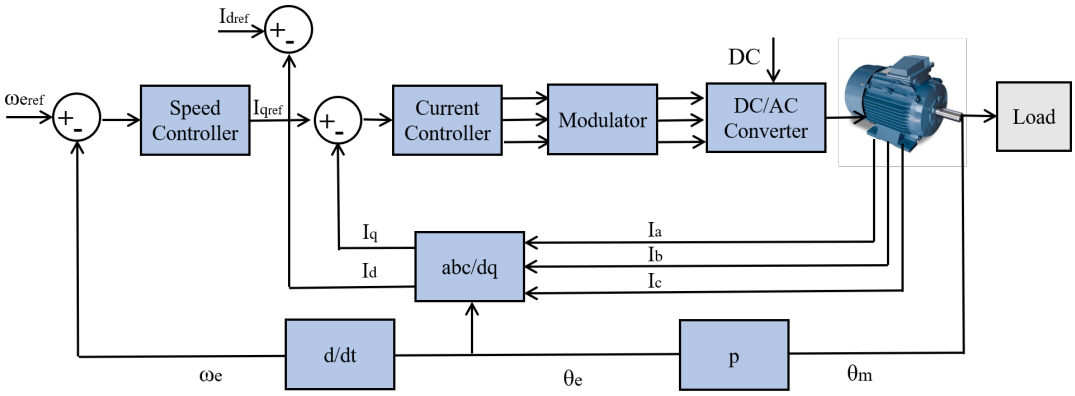

Figure 1.15: Control diagram of SM.

The required AC voltages are supplied using VSCs, governed by modulation techniques that generate a pulsating output voltage.

1.4.2 Applied PWM scheme

The armature's required voltage (desired magnitude, frequency, and angle) is calculated in the previous part to achieve the desired speed and torque references These voltages can be produced using a 3-phase VSC, shown in Fig. 1.16, using PWM techniques such as SWPM, SVPWM, and DPWM.

SPWM will be investigated analytically as proof of concept, but the principles for other modulation techniques are similar to SPWM. SPWM is established by comparing a high-frequency triangular carrier signal and a fundamental (modulating) signal. This fundamental signal is the reference signal of the motor, and the operating frequency of WPT is cultivated using the first harmonic of the carrier signal. The analytical model of SPWM can be obtained as given in (1.9), using double Fourier analysis.

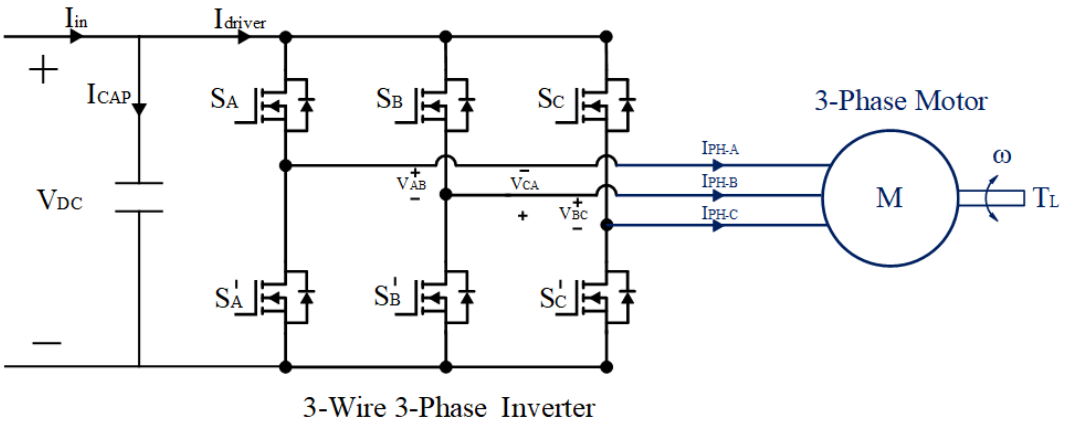

Figure 1.16: 3-phase 3-wire inverter

$$
\begin{aligned}
S = & \frac{1}{2} + \frac{m_a}{2}\cos\left(\omega_o t + \theta_o\right) \\
& + \frac{2}{\pi}\sum_{i=1}^{i=\infty} J_o\left(i\frac{\pi}{2}m_a\right)\sin\left(i\frac{\pi}{2}\right)\cos\left(i(\omega_c t + \theta_c)\right) \\
& + \frac{2}{\pi}\sum_{i=1}^{i=\infty}\sum_{k=-\infty}^{k=\infty}\left(\begin{array}{c} \frac{1}{i}J_k\left(i\frac{\pi}{2}m_a\right)\sin\left((i+k)\frac{pi}{2}\right) \\ \cos\left(i(w_c t + \theta_c) + k(w_o t + \theta_o)\right) \end{array}\right)
\end{aligned}
\tag{1.9}
$$

There are four main components for each leg: DC, fundamental, switching harmonics, and sidebands. The switching harmonics and their sidebands cannot be adjusted independently, and they change along with the modulation index, which linearly controls the magnitude of the fundamental frequency. Moreover, the phase angles of these components vary for each leg of the inverter, and they have positive, negative, or zero sequences, as shown in Table 1.1.

1.4.2.1 Control Methodology for the Proposed System

In the proposed system, a WPT-CSR is connected to a 2-wire of the 3-phase 3-wire motor drive, as given in Fig. 1.17. The normalized line-to-line voltage harmonics are given in Fig. 1.18. Since the switching harmonic is zero-sequence in conventional SPWM, it disappears in the line-to-line connection. Therefore, the line-to-line connected WPT-CSR is excited only by the sideband components. Additionally, the

Table 1.1: The sequences of fundamental frequencies, switching, and its sideband harmonics for inverter legs.

Frequency	Leg A	Leg B	Leg C	Sequence
f_o	0^o	120^o	-120^o	Positive
$f_s - 2f_o$	0^o	120^o	-120^o	Positive
f_s	0^o	0^o	0^o	Zero
$f_s + 2f_o$	0^o	-120^o	120^o	Negative

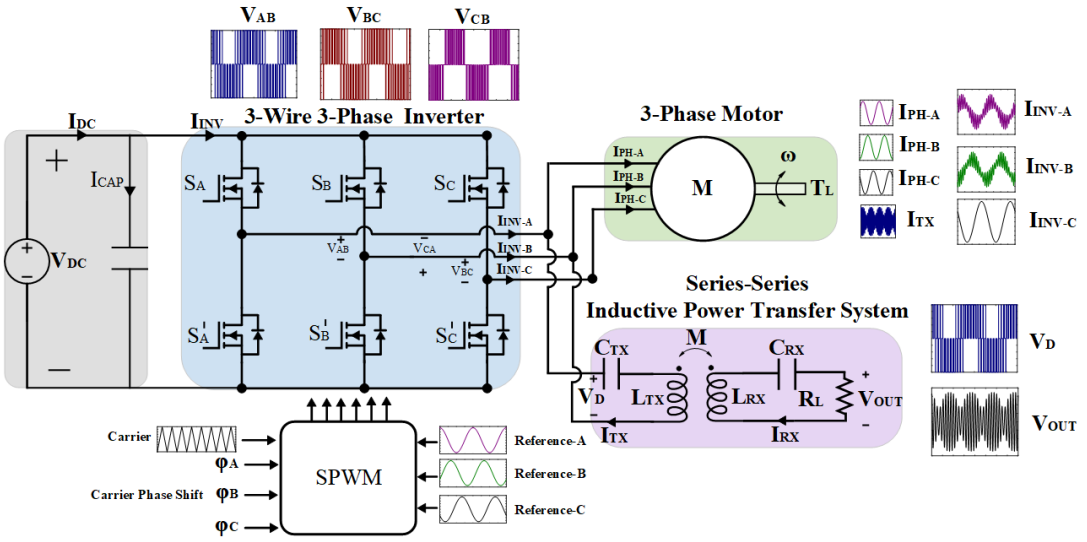

Figure 1.17: The circuit diagram of a single inverter system, which drives concurrently $3W$-3Φ motor and WPT system.

magnitude of these sideband components changes along with the modulation index, so it can not provide continuous power of WPT-CSR. This problem can be solved in different ways. Firstly, to regulate the WPT-CSR power, a post-regulation converter can be added to the receiver, increasing cost and complexity. Secondly, frequency detuning can be applied like DC motor drives. However, frequency detuning cannot guarantee to transfer of power under each modulation index (m_a) since sideband components converge to zero as m_a comes up to zero. In other words, the transferred power of the WPT system is decreasing while m_a is nearing zero. This diminished power is undesirable since the WPT-CSR may require the rated power for each operating condition of the motor. Finally, it is proposed that these problems can be solved

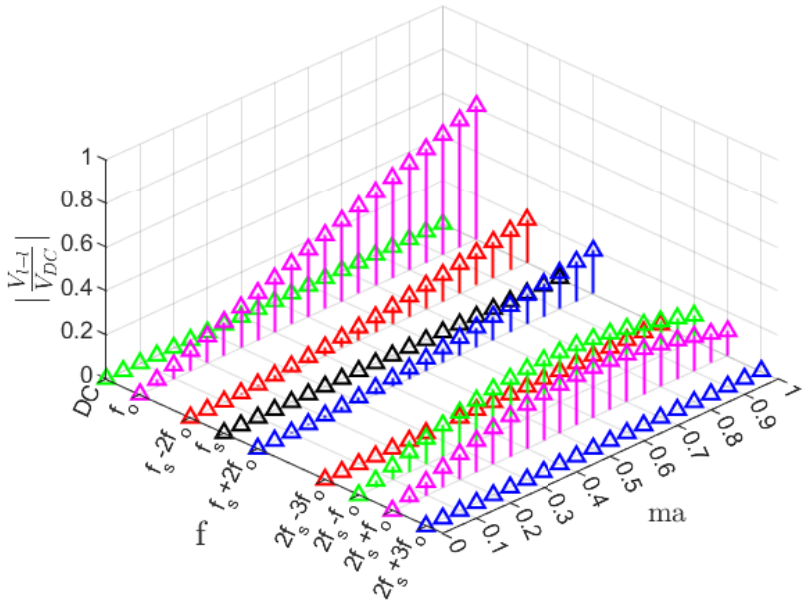

Figure 1.18: The harmonic distribution of a line-to-line voltage among different modulation indices without carrier phase shift.

by giving a phase shift between carrier signals of two legs. As can be seen from the double Fourier analysis in (1.9), phase angles of switching frequency and sidebands change as a function of the phase angle of the carrier signal. In this study, for the coherency, formulations will be made considering that the WPT-CSR is connected between legs A and B, and a carrier phase shift is given to leg B, as given in (1.10).

$$Carrier\ phases \begin{cases} \phi_{cA} = 0 \\ \phi_{cB} = \phi_{CPS} \\ \phi_{cC} = 0 \end{cases} \tag{1.10}$$

The magnitudes of switching frequency and sideband harmonics vary as given in (1.11, 1.12, 1.13). Thus, we can adjust the magnitude of each component by giving a proper carrier phase shift.

$$V_{sl}(m_a) = \frac{2}{\pi} J_2\left(m_a \frac{\pi}{2}\right) \sqrt{1 - cos(\phi_{CPS} + 120^o)} \tag{1.11}$$

$$V_s(m_a) = \frac{2}{\pi} J_o\left(m_a \frac{\pi}{2}\right) \sqrt{1 - cos(\phi_{CPS})} \tag{1.12}$$

$$V_{sh}(m_a) = \frac{2}{\pi} J_2\left(m_a \frac{\pi}{2}\right) \sqrt{1 - cos(\phi_{CPS} - 120^o)} \tag{1.13}$$

These magnitudes can be plotted for variable carrier phase shifts and modulation indices, as shown in Fig. 1.19.

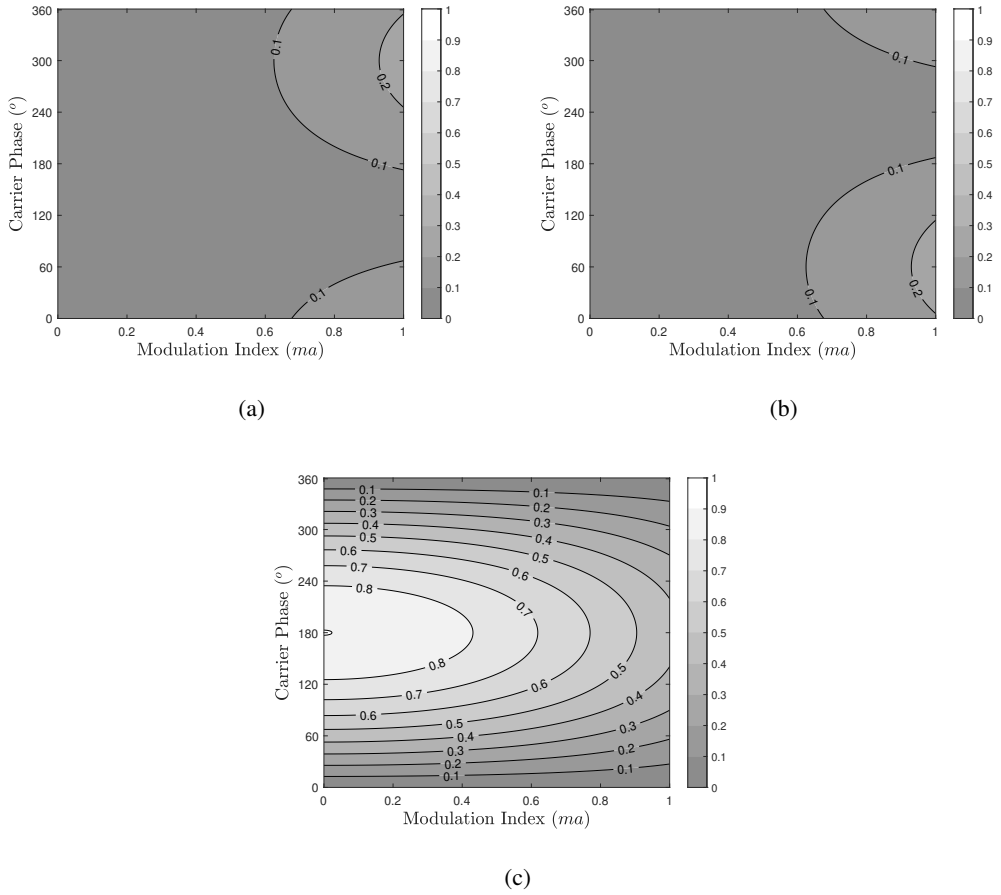

Figure 1.19: Normalized inverter ouput voltages $|\frac{V_{l-l}}{V_{DC}}|$. (a) Lower sideband of the switching frequency (f_{sl}). (b) Switching frequency (f_s). (c) Higher sideband of the switching frequency (f_{sh}).

A challenge is to determine the amount of the phase shift, which must guarantee a constant power transfer for any modulation indices. As shown in Fig. 1.19, while the magnitude of the switching frequency harmonic increases by increasing CPS, the magnitude of the sidebands decreases. Considering the quality factor of WPT-CSR, the gain of the switching frequency and its sideband harmonics are nearly equal since their frequencies are close enough. Instead of investigating each component in the

time domain, we can build an equivalent drive voltage assuming all components to have the same frequency. The RMS equivalent drive voltage (V_D) can be calculated using (1.14) since all these frequencies are orthogonal to each other.

$$V_D = \sqrt{\left(V_{sl}^2 + V_{sw}^2 + V_{sh}^2\right)} \tag{1.14}$$

Using the equivalent center harmonic approach, a normalized drive voltage is shown

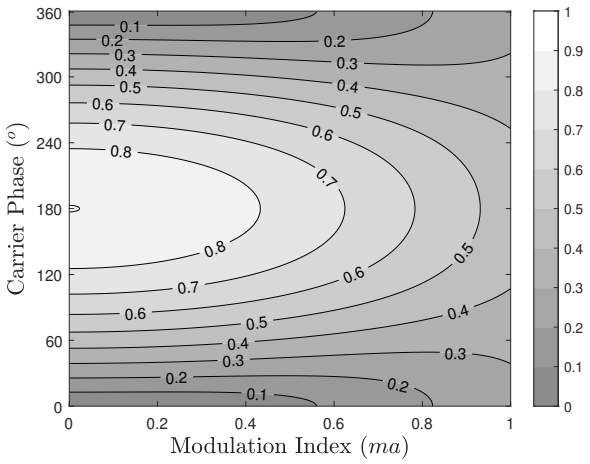

Figure 1.20: Normalized inverter output voltages $|\frac{V_{l-l}}{V_{DC}}|$ using the center harmonic approach.

for various carrier phase shifts and modulation indices in Fig. 1.20. As can be seen, for each modulation index, we can guarantee the normalized gain between 0.25 and 0.45 by keeping the carrier phase shift between 30^o and 60^o. While the carrier phase shift is approaching 180^o, the normalized drive voltage increases. However, at this point, we cannot fully control the voltage level; for example, the drive voltage acquired at $m_a = 0$ cannot be reached at $m_a = 1$.

Consequently, the control diagram for the proposed system is given in Fig. 1.21. The motor controller decides on the modulation index, considering the desired speed and torque references. Then, the WPT-CSR controller adjusts the carrier phase shift to obtain the desired WPT-CSR output power for these different motor operations.

The key voltage and current waveforms without and with CPS are given in Fig. 1.22 and Fig. 1.23 respectively. While the fundamental signal is determined by modulating signals, the switching frequency and its sidebands are controlled by CPS.

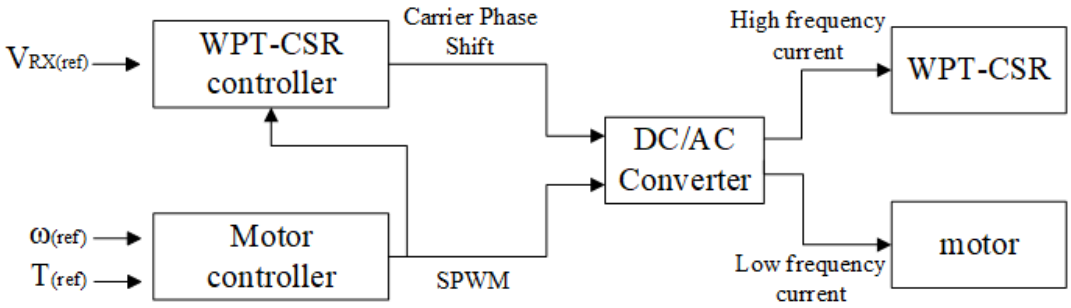

Figure 1.21: The block diagram of the control method of the combined motor and IPT system.

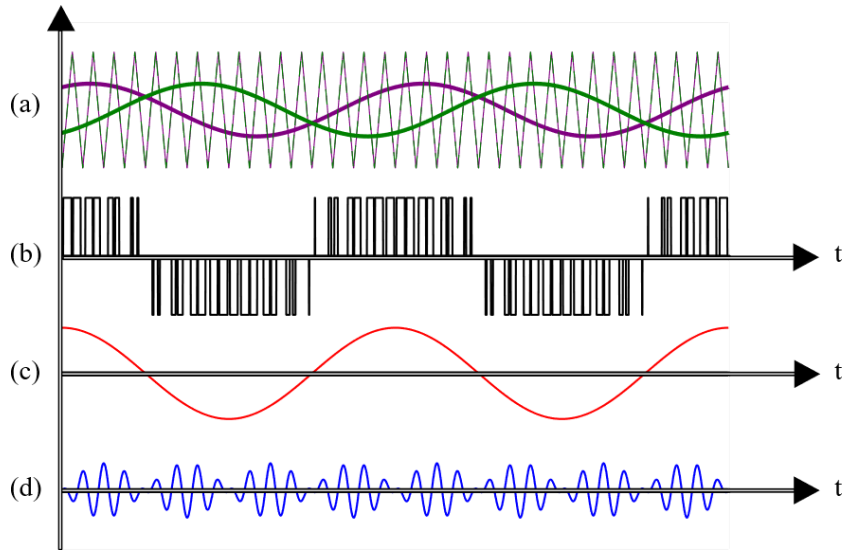

Figure 1.22: Key waveforms without CPS. (a) Ph-A (purple) and Ph-B(green) carrier triangles and sinusoidal references. (b) Line-to-line voltage of ph-A and ph-B (V_{AB}). (c) The waveform of fundamental frequency of (V_{AB}). (d) The waveform of the switching frequency and its sidebands of (V_{AB}).

1.5 Current Modulation Techniques of Conventional Drives

Many modulation techniques for DC and AC motors are used in industrial motor drives. While SPWM, SVPWM, and DPWM are prevalent for AC motor drives, unipolar-PWM and bipolar-PWM are prevailing for DC motor drives. Each modulation technique has its advantages. For example, while SVPWM effectively utilizes the DC link voltage, DPWM provides reduced switching losses. Unipolar PWM has

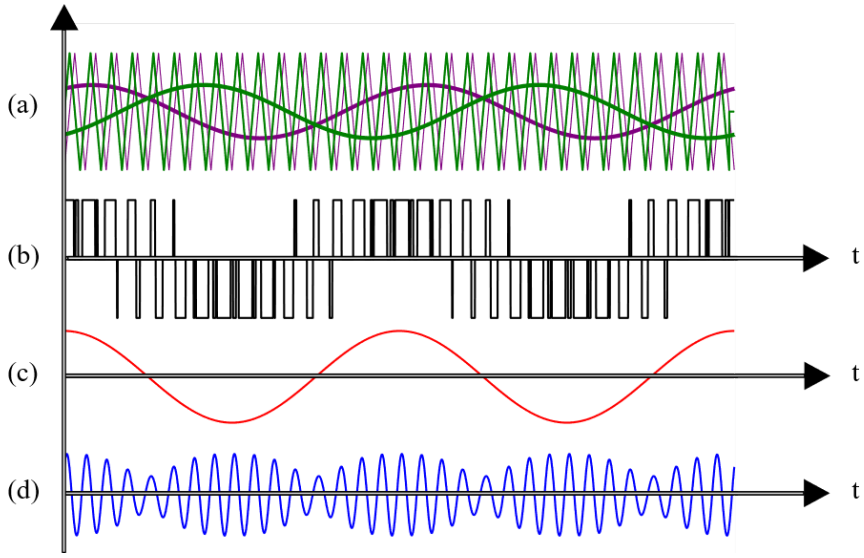

Figure 1.23: Key waveforms with CPS. (a) Ph-A (purple) and Ph-B(green) carrier triangles and sinusoidal references. (b) Line-to-line voltage of ph-A and ph-B (V_{AB}). (c) The waveform of fundamental frequency of (V_{AB}). (d) The waveform of the switching frequency and its sidebands of (V_{AB}).

lower switching harmonics than bipolar PWM. Although the proposed system is implemented with bipolar PWM and SPWM respectively for DC and AC motors, it can also be applied with other modulation techniques. For example, the change

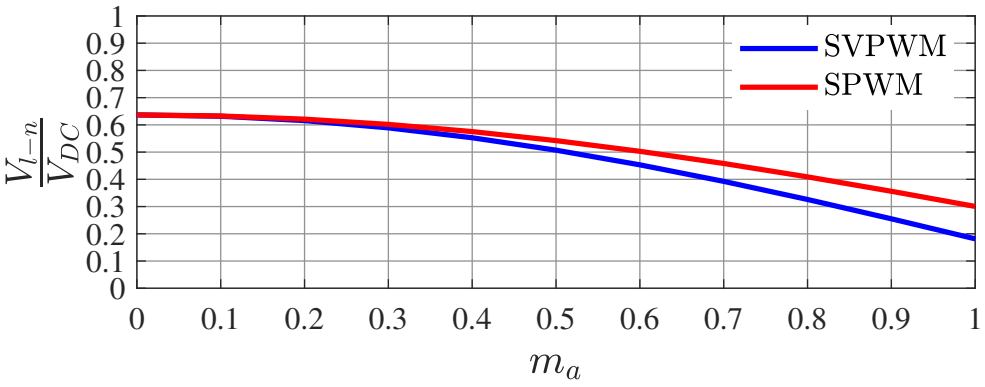

Figure 1.24: The normalized inverter voltage ($\frac{V_{l-n}}{V_{DC}}$) of the switching harmonics over modulation indexes (m_a)

in the magnitude of the switching frequency over modulation indices is presented in Fig. 1.24 for SPWM and SVPWM. It is observed that the tendency of the magnitude

of the switching harmonic of SVPWM is similar to SPWM, and it can be controlled in line-to-line connection via the proposed CPS as presented before.

1.6 Practical Considerations

For conventional industrial motor drives, the switching frequency is usually below 20 kHz due to the switching losses of silicon (Si)-based transistors [2]. WPT-CSR is not feasible in this frequency range since the Tx-Rx coils get bulkier as the frequency is reduced [3]. The relation between the size of the coil and switching frequency is shown in Fig. 1.25. However, recent developments in semiconductor technology

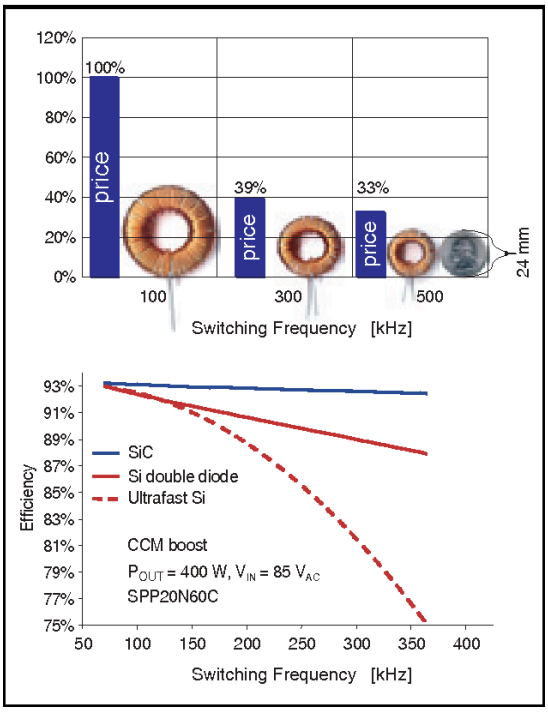

Figure 1.25: Switching frequency and power capabilities of the semiconductors for the converters [1]. (Figure degistirilecek :))

pave the way for higher switching frequencies (up to several hundred kHz), with Silicon Carbide (SiC) or Gallium Nitride (GaN) based motor drives [4, 5] while still achieving high efficiency [6]. The switching frequencies and power capabilities of different semiconductor technology are given in Fig. 1.26.

Consequently, choosing a proper switching frequency is challenging since a high

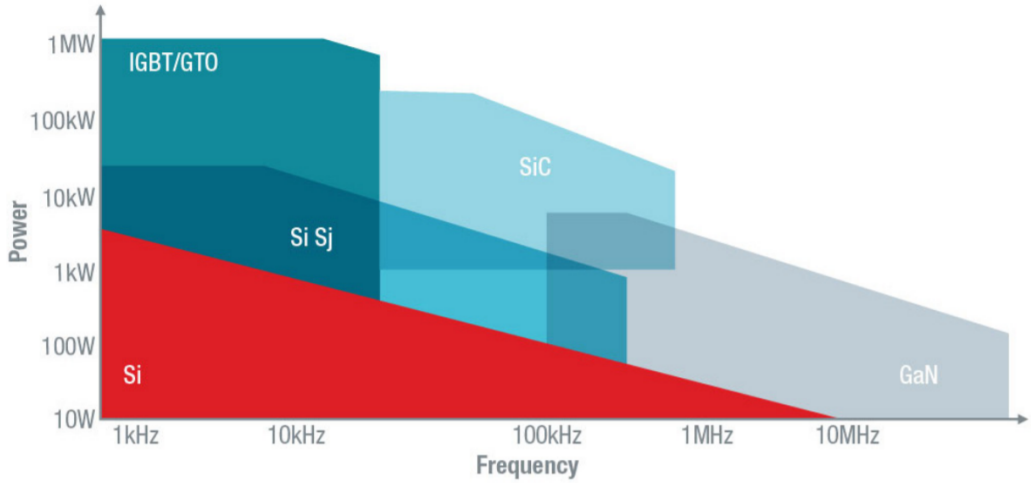

Figure 1.26: Switching frequency and power capabilities of the semiconductors for the converters [1].

switching frequency increases the converter losses, and a low switching frequency increases the coil size and cost. With the development of wide band-gap devices, a sweet spot could be found, satisfying both requirements. Thus, it is now possible to utilize the wide band-gap drives as a single converter for concurrent operations.

REFERENCES

[1] "Finding the right power supply technology for your design,edn," 2018.

[2] S. Tiwari, O. . Midtgård, and T. M. Undeland, "Sic mosfets for future motor drive applications," in *2016 18th European Conference on Power Electronics and Applications (EPE'16 ECCE Europe)*, pp. 1–10, 2016.

[3] V. Shevchenko, O. Husev, R. Strzelecki, B. Pakhaliuk, N. Poliakov, and N. Strzelecka, "Compensation topologies in ipt systems: Standards, requirements, classification, analysis, comparison and application," *IEEE Access*, vol. 7, pp. 120559–120580, 2019.

[4] A. K. Morya, M. C. Gardner, B. Anvari, L. Liu, A. G. Yepes, J. Doval-Gandoy, and H. A. Toliyat, "Wide bandgap devices in ac electric drives: Opportunities and challenges," *IEEE Transactions on Transportation Electrification*, vol. 5, no. 1, pp. 3–20, 2019.

[5] W. Lee, S. Li, D. Han, B. Sarlioglu, T. A. Minav, and M. Pietola, "A review of integrated motor drive and wide-bandgap power electronics for high-performance electro-hydrostatic actuators," *IEEE Transactions on Transportation Electrification*, vol. 4, no. 3, pp. 684–693, 2018.

[6] E. A. Jones, F. F. Wang, and D. Costinett, "Review of commercial gan power devices and gan-based converter design challenges," *IEEE Journal of Emerging and Selected Topics in Power Electronics*, vol. 4, no. 3, pp. 707–719, 2016.